Contrasting the role of regional and remote circulation in driving Asian monsoon biases in MetUM GA7.1

Article

Accepted Version

Liu, Z., Bollasina, M. A., Wilcox, L. J. ORCID: https://orcid.org/0000-0001-5691-1493, Rodriguez, J. M. and Regayre, L. A. (2021) Contrasting the role of regional and remote circulation in driving Asian monsoon biases in MetUM GA7.1. Journal of Geophysical Research: Atmospheres, 126 (14). e2020JD034342. ISSN 2169-8996 doi: https://doi.org/10.1029/2020JD034342 Available at https://centaur.reading.ac.uk/99212/

To link to this article DOI: http://dx.doi.org/10.1029/2020JD034342

Publisher: American Geophysical Union

Contrasting the role of regional and remote circulation in driving Asian monsoon biases in MetUM GA7.1

Zhen Liu[1], Massimo A. Bollasina[1], Laura J. Wilcox[2,3], José M. Rodríguez[4], and Leighton A. Regayre[5]

[1] School of GeoSciences, University of Edinburgh, UK
[2] National Centre for Atmospheric Science, UK
[3] Department of Meteorology, University of Reading, Reading, UK
[4] Met Office, Exeter, UK
[5] Institute for Climate and Atmospheric Science, School of Earth and Environment, University of Leeds, Leeds, UK

Corresponding author: (z.liu@ed.ac.uk)

Key Points:

- Nudging can substantially reduce precipitation biases.
- Seasonal precipitation biases over India and eastern China are mostly driven by local circulation except over eastern China in summer.
- Nudging improves the simulated El Niño teleconnections to India and China and monsoon onset date in particular over India.

Key words: monsoon biases, nudging, regional circulation, remote circulation

Abstract

Monsoon precipitation affects nearly half of the world's population, but monsoon biases are a long-standing problem in climate simulations. We apply dynamical nudging either globally or regionally to demonstrate the role of regional and remote circulation in generating Asian monsoon biases in an atmospheric general circulation model. Monsoon precipitation biases are substantially reduced in response to global nudging but may also be exacerbated over the warm oceanic equatorial areas because of unconstrained sub-grid convection. Regional nudging over Asia appears to be more efficient than nudging outside Asia in reducing seasonal precipitation biases over eastern China and India. This suggests a predominant role of local circulation anomalies in generating monsoon precipitation errors in these regions. An exception is the summer precipitation bias over eastern China, which is more strongly controlled by remote circulation. Besides seasonal mean rainfall, nudging can also improve the simulated interannual and intraseasonal precipitation variability over the subtropics. This results in a better skill in reproducing the observed El Niño teleconnections to India and China and the monsoon onset date. Improved understanding of the origin of Asian monsoon biases and the contribution from regional and remote circulation advances our knowledge of the interplay between the Asian monsoon and large-scale circulation, which can be beneficial to the simulation and interpretation of monsoon projections.

1 Introduction

The Asian monsoon is a key component of the global atmospheric circulation. During the summer, the monsoon southerlies provide around two thirds of the annual precipitation to about half of the world's population, while during the winter northerly winds can lead to cold surges and severe weather (e.g., Li & Yang, 2010; Wang 2006). Given the complexity and spatial extent of the monsoon, its simulation has proven to be a challenging task for climate models, as well as a key testbed to evaluate their processes (Sperber et al., 2013).

Numerous studies have documented the model monsoon biases, as well as their spatio-temporal evolution with the annual cycle (e.g., Kang and Shukla, 2006; Zhou et al., 2009). Many of these shortcomings have been persisting for decades (Ramesh and Goswami, 2014; Song and Zhou, 2014a). These include the excessive summer rainfall over the northwestern Pacific associated with an anomalously weak Western Pacific Subtropical High (WPSH), and a dipole precipitation anomaly over the Indian monsoon region with a rainfall deficit over the subcontinent and excess precipitation over the tropical Indian Ocean (e.g., Rodríguez et al., 2017; Sperber et al., 2013). The pervasiveness of these biases across both coupled and uncoupled models (Bollasina and Nigam, 2009; Song and Zhou, 2014b) suggests the underlying causes could be rooted in their atmospheric component. However, there is some evidence that coupled models can better reproduce monsoon precipitation than atmosphere-only models (Kumar et al., 2005; Zou, 2020) from two main reasons: the damped atmospheric interval variability due to negative feedback from the ocean (Zhou et al., 2018) and the compensating effects between atmospheric and sea surface temperature (SST) biases (Prodhomme et al., 2014; Yang et al., 2019).

Model biases hinder reliable attribution of past monsoon variations to anthropogenic forcing (e.g., Wilcox et al., 2015), which in turn hampers our confidence in future projections. One of the limiting factors is the interaction between external forcing and internal variability, especially at interannual to decadal time scales (e.g. Deser et al. 2012). Large uncertainties stem from the atmospheric dynamical response (Shepherd, 2014), which is particularly crucial for the Asian monsoon as the large-scale circulation exerts a strong control on Asian climate (Chen et al., 2000). However, large discrepancies exist in the model representation of key circulation characteristics, such as the WPSH (Liu et al., 2014), the East Asian trough (Wei et al., 2014), and the cross-equatorial flow over the western Indian Ocean (Bollasina and Nigam, 2009). Even within the climatological seasonal cycle, our understanding of the interplay between the Asian monsoon and the large-scale tropical and extratropical circulation, and how this influences model biases is far from complete (e.g. Zhou et al. 2016). Addressing these knowledge gaps is critical to reduce uncertainties in future projections of regional water availability over Asia.

One approach to reduce the effect of circulation biases is nudging (also known as Newtonian relaxation). By constraining the model large-scale circulation toward reanalysis, nudging can be used to estimate errors in local sub-grid processes (e.g., convection and topography; Telford et al., 2008; Eden et al., 2012). Nudging can also aid the detection of forced signals by constraining natural variability (e.g., Johnson et al., 2019; Kooperman et al., 2012; Lin et al., 2016; Regayre et al., 2014). However, biases may not necessarily decrease with nudging (e.g., Kooperman et al., 2012) as the forcing by the additional relaxation terms may potentially drive the model away from its balanced state (Wehrli et al., 2018).

Only few recent studies have investigated the effect of nudging on the simulation of the Asian monsoon, showing that South Asian and Maritime Continent (MC) precipitation biases are closely linked to circulation biases over East Asia and the western Pacific (Rodríguez et al., 2017; Rodríguez and Milton, 2019). Yet, the extent to which nudging over different regions contributes to improving the monsoon simulation, and the underlying mechanisms showing potential for reducing monsoon biases, have not been investigated in a consistent way.

2 Data and Methods

We use version 7.1 of the atmospheric component of the Met Office Unified Model (MetUM GA7.1), which includes significant improvements to the convection and aerosol schemes compared to GA6 (Mulcahy et al., 2018; Williams et al., 2018). The model is run at N96 horizontal resolution (1.25° x 1.875° in latitude and longitude, respectively), with 85 vertical levels up to 85 km (Walters et al., 2019). Daily observed SST and sea ice concentration are taken from the European Centre for Medium-Range Weather Forecasts (ECMWF) Interim reanalysis (ERA-I; Dee et al., 2011). Monthly emissions of anthropogenic aerosols and their precursors are prescribed following CMIP6 (Hoesly et al., 2018).

We performed a set of five experiments (see Table 1) for the period December 1991 – December 2012, driven by the same external forcing and surface boundary conditions. The control experiment (CONT), in which the atmospheric model is evolving freely (AMIP-like), is complemented by four simulations with horizontal winds relaxed toward ERA-I with a 6-hourly time scale. In three of these simulations, nudging is applied only above the planetary boundary layer (model level 12, or approximately 850 hPa), which constrains the large-scale circulation and allows low-level winds to adapt to local surface conditions (Telford et al., 2008). In particular, winds are nudged either globally (GLOB) or only over part of the domain, i.e. over or outside Asia (ASIA and ELSE, respectively; Asia is the region 10°–45°N, 60°–125°E marked by the purple box in Fig. 1a). The comparison of ASIA and ELSE to GLOB is used to isolate the role of local and remote circulation biases on the simulated monsoon. A fifth experiment with winds nudged globally throughout the whole atmospheric column (GLOB_A) was performed to explore the effect of constraining the circulation in the boundary layer.

Three ensemble members, initialised from different atmospheric conditions, were run for CONT and ELSE to test whether internal variability may influence the results. A comparison between the different ensemble members shows marginal differences in precipitation and winds (Fig. S1), indicating that one member is sufficient to isolate the monsoon biases out of internal variability. Note that temperature is not nudged to prevent the appearance of spurious diabatic heating and precipitation anomalies (e.g. Zhang et al. 2014); the effect of additional temperature nudging is briefly discussed in Section 4.

The seasonal mean in both winter (December – February) and summer (June – August) and sub-seasonal features at monthly and pentad scales are analyzed for the last 20 simulated years (the first year is discarded as spin-up). The model precipitation is evaluated against the average of the Global Precipitation Climatology Project (GPCP) version 2 (Adler et al., 2003) and the Climate Prediction Center Merged Analysis of Precipitation (CMAP; Xie & Arkin, 1997) datasets, while ERA-I is used to assess the simulated three-dimensional circulation. We use the non-parametric Kolmogorov-Smirnov test to evaluate the significance of the differences between the nudged simulations and observations. The significance of the regression coefficients is estimated by the Student's *t* test.

The simulated interannual variability (IAV) of precipitation is calculated as the standard deviation of the 20-year long time series of summer mean precipitation at each grid point, while intraseasonal variability (ISV) is computed as the standard deviation of the 20–90-day Butterworth bandpass filtered pentad time series (Russell, 2006), after removing the annual cycle (the time mean and the first three harmonics). We also examined the effect of nudging on the El Niño-monsoon teleconnections and monsoon onset, which are well linked to IAV and ISV, respectively. The relationship between El Niño and the summer monsoon is diagnosed by the simultaneous regressions of precipitation and 925-hPa winds onto the Niño3.4 index using seasonal mean values (Wang et al., 2000). Following Wang and Ho (2002), the onset date is defined as the first pentad of the rainy season whose mean precipitation exceeds 5 mm/day above the corresponding January mean precipitation rate over the monsoon domain.

3 Results

3.1 Monsoon biases in the control experiment

Fig. 1 shows the precipitation and low-level circulation biases in CONT, as well as their link via vertically-integrated (surface to 300 hPa) stationary moisture fluxes and 200-hPa divergent circulation biases. To provide context, Fig. S2 displays the corresponding observed climatology.

In the winter, CONT exhibits a substantial dry bias (above 3 mm/day) over a large area covering the eastern Indian Ocean and the MC (Fig. 1a). Conversely, prominent rainfall excess (up to 5 mm/day) is found over the central and western Indian Ocean and the western Pacific between 30°S and 10°N, with a maximum over the South Pacific Convergence Zone (SPCZ). Albeit of small magnitude, model wet biases over India and eastern China are substantially larger than climatological values (+157% and +70%, respectively, in Table 2). The regions used to compute area-mean biases are displayed in Fig. S3.

Accompanying the winter precipitation biases are errors in the simulated lower-tropospheric circulation. A large anticyclonic bias over the northwestern Pacific is associated with an eastward extension of the Siberian High as well as a weaker Aleutian low. This induces a strong moist easterly flow across the warm subtropical Pacific (Fig. 1a), which bifurcates over the southern Philippines Sea. One branch reaches eastern China, opposing the drier climatological northeasterlies (Fig. S2a), and then continues across Indochina and the northern Bay of Bengal (BOB), weakening the climatological northwesterlies and bringing moisture to India. The other branch turns anticlockwise approaching the equator, contributing to the northwesterly bias from the MC to the SPCZ. To the west of the MC, a strong easterly bias and moisture transport from the MC across the Indian Ocean are associated with a stronger and northeastward displaced Mascarene High, counteracting the climatological westerlies (Fig. S2a). These features are linked via anomalous three-dimensional circulation cells both in the zonal (Walker-type) and meridional directions (e.g., Neale & Slingo, 2003; Toh et al., 2018). For example, the dry MC bias and corresponding subsidence is associated with upper-tropospheric inflow from the divergence centers over the Indian and western Pacific Oceans, where increased ascent and excess rainfall occur (Fig. 1e).

During the summer, the precipitation bias features a quadrupole with positive anomalies over the equatorial Indian Ocean and the northwestern subtropical Pacific, and drying over the Indian subcontinent and the MC (Fig. 1b). An anomalous near-surface anticyclone over northern India weakens the climatological southwesterly moisture transport from the Arabian Sea and leads to the dry bias over India. The associated northerlies together with enhanced south-equatorial southerlies from a stronger Mascarene high circulation converge along the equatorial Indian Ocean, generating the local rainfall maximum. To the east, the model simulates a weaker WPSH, a common bias across CMIP5 models (e.g., Liu et al., 2014; Wilcox et al., 2015), resulting in anomalous northeasterly wind and weaker moisture transport over central China (Fig. 1d). Albeit spatially confined, rainfall reduces over the Yangtze River basin (10% over 28°–34°N, 110°–125°E). Meanwhile, stronger moist westerlies blow from the BOB across Indochina to the South China Sea and the Northwestern Pacific, where they converge with the northward divergent flow from the MC, leading to enhanced precipitation. A quadrupole structure is also manifest in the 200-hPa stream function bias (not shown), which features a pair of cyclones over the Indian Ocean south and north of the equator, and a pair of anticyclones over the western subtropical Pacific, with the northern hemispheric one particularly extensive. This pattern (and its low-tropospheric counterpart, of baroclinic nature) bears the imprint of a Gill-Matsuno-type response to suppressed diabatic heating over the BOB, similar to the large-scale anomalies associated with perturbed South Asian monsoon heating in idealised baroclinic models (e.g. Lin, 2009; Sardeshmukh & Hoskins, 1988).

The coupled zonal and meridional vertical circulations in the summer make identifying the region driving the overall bias pattern across the Indo-Pacific sector less clear. Examination of the 200-hPa divergent circulation bias may provide insights into the existence and strength of such links (Fig. 1f). A strong outflow from the equatorial Indian Ocean is directed toward South Asia and the eastern north equatorial Indian Ocean, consistent with the meridional overturning circulation between the two areas (e.g., Nigam and Chan 2009). The 200-hPa inflow over South Asia displays an appreciable contribution from ascent and subsequent upper-tropospheric divergence over the western subtropical Pacific and further to the east, associated with the expansive anomalous cyclone and precipitation increases (Fig. 1b). A transverse meridional circulation cell is also recognisable between the western subtropical Pacific and the equatorial MC and the SPCZ (Fig. 1f), consistent with the reciprocal influence of the two areas found in Nigam and Chan (2009) and Lin (2009). Note the link between the eastern sub-equatorial Indian Ocean and the eastern MC appears to be comparatively weak with smaller divergent wind biases, as opposed to the strong zonal circulation during the winter, suggesting their direct influence to be modest.

3.2 Effect of global nudging above boundary layer on the monsoon biases

Fig. 2 displays the differences in precipitation and 925-hPa winds between the four nudged simulations and observations (refer to Fig. S4 for the corresponding differences with respect to CONT). In the winter, GLOB features a reduction in the meridional extent of areas with large precipitation excess compared to observations. Relative drying of the tropics, particularly in the Southern Hemisphere, is partially compensated by enhanced oceanic rainfall near the equator where warmer climatological SSTs are found (Figs. 1a and 2a). This manifests as a northward precipitation shift over both the Indian Ocean and the SPCZ, each associated with an extensive anomalous near-surface subtropical cyclone to the east and wind convergence on its western flank (Fig. S4a). The resulting anomalous westerlies across the equatorial Indian Ocean converge with south-westerlies over the SPCZ, opposing the CONT wind biases and leading to a reduction in the dry bias over the MC by 0.7 mm/day (Table 2).

Nudging substantially improves the simulated circulation in the north-western extratropical Pacific by counteracting the extensive anticyclonic bias (Fig. 2a). This results in anomalous dry northwesterlies over northern India and westerlies over eastern China and the northern South China Sea (Fig. S4a), opposing CONT winds of oceanic origin, considerably alleviating the wet biases there (152%, 32%, and 25%, respectively, in Table 2). The winds, turning to northerlies approaching the equator, converge with the southern hemisphere southerlies, generating the north-equatorial Pacific rainfall excess (Fig. 2a). Inspection of the 200-hPa divergent flow shows a much smaller inflow toward the MC, suggesting an anomalous divergent outflow caused by nudging (Fig. 3a). The strongest outflow is directed northeastward to the subtropical western Pacific Ocean (Fig. S5a), leading to strengthening of the WPSH and establishment of a vigorous meridional overturning cell. This suggests a strong influence of the abatement of the MC rainfall bias on the model shortcomings over the surrounding Asian-Pacific region, likely related to an improved local circulation associated with land-sea breezes and the diurnal cycle. The unrealistic representation of these local features related to the complex terrain is the main reason for precipitation biases over the MC in climate models (Im & Eltahir, 2018).

During the summer, the amplitude of the quadrupole pattern biases is drastically reduced across the Indo-Pacific sector in GLOB (Fig. 2b). This indicates a general reduction of the model bias except for a reversal over the northern South China Sea, and hints to the existence of a common factor driving the regional rainfall distribution. Other exceptions are the south-equatorial Indian Ocean and the double intertropical convergence zone (ITCZ) region, where rainfall further increases. A plausible physical mechanism will be discussed later in this section.

The strong and extensive anomalous cyclone bias almost disappears over the western Pacific in GLOB, denoting a substantial enhancement in the simulated WPSH (Fig. 2b), with a marked reduction of the wet bias by 5.6 mm/day (Table 2). On the southwestern flank of the anomalous anticyclone induced by nudging, strong easterlies oppose the CONT westerly bias, resulting in large moisture transport from the South China Sea across Indochina and the BOB toward India relative to CONT (Fig. S4b). This leads to a reversal of the CONT wet bias over northern Indochina and the northern South China Sea (from +2.0 mm/day to –2.2 mm/day over 12°–22°N, 100°–120°E; Fig. 2b). Although the easterly anomalies oppose the climatological westerly winds over India, they converge with the westerly anomalies associated with the equatorial Indian Ocean dry anomalies (Fig. S4b), resulting in a considerable reduction of the dry bias over Indian land areas (Table 2). Additionally, a stronger southerly moisture transport over eastern China makes GLOB wetter than CONT over eastern China, reversing the CONT dry bias over the Yangtze River basin (from –0.6 mm/day to +1.0 mm/day in Table 2).

GLOB substantially reduces the average summertime dry bias over the MC by 1.4 mm/day (Table 2). Note that in GLOB the biases in the MC precipitation and near-surface winds have more spatial variations compared to CONT (Figs. 1b and 2b), possibly associated with a more realistic representation of local circulation and convection. The emergence of local effects is evident in the details of the rainfall pattern. For example, while closer to observations, rainfall remains biased low over the islands with nudging, yet it is biased high over the ocean grid-points.

The difference in the 200-hPa divergent flow between GLOB and observations features a clear alleviation of convergent flow bias toward South Asia during boreal summer, particularly over the southern BOB (Fig. 3b). In response to global nudging, the bulk of the flow heads northwestward, similar to the monsoon-desert mechanism (Rodwell & Hoskins, 1996), and northeastward toward the northwestern Pacific and even further downstream toward the central basin (Fig. S5b). Albeit weaker, the southward link with the equatorial Indian Ocean is also evident. There is also a strong overturning circulation apparent over the MC and the western subtropical Pacific. Besides, these two main structures of the upper-tropospheric divergent flow display some degree of zonal coupling (e.g., between the eastern MC and the central equatorial Indian Ocean).

The MC is at the centre of circulation differences between GLOB and CONT (Fig. S5b), but there are complex changes in the diabatic heating distribution over this deep convective region, which are conflated with strong vertical circulations in the wider Indo-Pacific region (Jiang et al., 2016). Thus, isolation of the influence of the biases over the individual sub-regions in generating the overall pattern displayed in Fig. S5b is a formidable task without the use of further sensitivity simulations. Some conclusions can however be drawn from existing studies using idealised diabatic heating distributions with linear and more advanced models (e.g., Greatbatch et al., 2013; Jiang et al., 2016). Despite intrinsic differences in the model used and experimental settings among the various studies, it is possible to speculate that the MC has a predominant influence on the subtropical western

Pacific, while South Asia has an important influence on the Indian Ocean as well as to the east over China and the northwestern tropical Pacific.

Overall, the comparison between GLOB and CONT shows that nudging markedly improves simulated precipitation over the Asian subtropics through a better representation of important seasonal and permanent circulation features (Figs. 1 and 2). However, the near equatorial positive rainfall bias may be exacerbated but more confined along the warm oceanic region with nudging despite a better simulated mid- and upper-tropospheric circulation (e.g., ITCZ). Several studies have emphasised the importance of unconstrained sub-grid convection due to the fact that it acts on shorter time scales than nudging (e.g., Lohmann & Hoose, 2009; Wehrli et al., 2018). Johnson et al. (2019) reported similar findings, albeit in the context of nudged experiments under black carbon forcing, and showed a strong circulation change over the tropics but suppressed dynamical adjustments in the mid-latitudes. A close examination of the positive near-equatorial rainfall bias in both CONT and GLOB (Figs. 1 and 2) suggests its location to be controlled both by the movement of the warm SSTs and by the convergence of near-surface winds associated with meridional SST gradients (Bollasina and Ming, 2013). This is evident over the Indian Ocean in winter for CONT (Fig. 1a), and in summer for GLOB (Fig. 2b), as well as over the western Pacific in winter for both experiments.

As in CONT, magnitude and spatial pattern of the precipitation bias relative to satellite observations (Fig. 2) broadly follow those in moisture flux convergence (MFC; Fig. S6), particularly over the tropical oceans, suggesting the small contribution from transient eddies. To explore possible reasons for the persistence of some precipitation biases after nudging the circulation globally, we decompose the MFC differences between GLOB and observations into dynamic and thermodynamic terms associated with variations in circulation and humidity, respectively, following Seager et al. (2010). The simulated bias in the dynamic contribution accounts for a large portion of the MFC biases and subsequent precipitation errors in both control and GLOB experiments (e.g., over the double ITCZ; Figs. S6 and S7) while the thermodynamic term is relatively small and shows no appreciable variations (not shown). This implies that a substantial part of the precipitation biases is generated through circulation changes rather than through changes in humidity regardless of whether nudging is applied or not. This argument is also valid for other nudged experiments.

3.3 Effect of additional nudging within the boundary layer

Nudging over the whole atmospheric column (GLOB_A) further constrains the low-level atmospheric circulation and thus may lead to a more realistic simulation of boundary layer processes. Note this too strong constraint is normally not recommended to enable the adjustments of low-level wind to surface conditions (Telford et al., 2008) and the radiative effects of short-lived climate forcers (e.g. aerosols; Regayre et al., 2018).

The broad features of the patterns of biases of winter precipitation and 925-hPa winds in GLOB_A are similar to those in GLOB (Figs. 2a and 2c). A notable difference is the further reduction of the CONT dry bias over the MC and the wet bias over the Indian Ocean and ITCZ associated with a more realistic wind distribution. These bias reductions are possibly related to an improved representation of land-sea breezes and their interaction with the complex topography of the region. The additional MC rainfall in GLOB_A compared to

GLOB results in stronger upper-tropospheric outflow (Figs. 4a and 4c). Not surprisingly, the corresponding near-surface return flow toward the MC features anomalous equatorial westerlies from the Indian Ocean and easterlies over the Pacific Ocean in GLOB_A compared to GLOB (Fig. 4a), further reducing the model easterly and westerly wind bias, respectively. Also, anomalous northerlies over eastern China lead to a reduction of the CONT wet bias there (Table 2). Conversely, stronger northwesterlies in GLOB_A than in GLOB over northern India, while largely alleviating the model southeasterly bias, lead to a weak dry bias.

The patterns of summer GLOB_A and GLOB precipitation and low-tropospheric wind bias are also similar (Figs. 2b and 2d). Inspection of the difference between GLOB_A and GLOB (Fig. 4b) reveals that additional boundary layer nudging reduces the equatorial wet bias in GLOB (Fig. 2b). The response pattern is dominated by increased rainfall and strong upper-tropospheric divergence over the central-eastern north-equatorial Indian Ocean and the western MC relative to GLOB (Figs. 4b and 4d). The divergent flow heads primarily in a zonal direction toward the western equatorial Pacific, where it converges and reduces the wet bias in the ITCZ region. The circulation response also shows a pair of meridional overturning cells in both the Indian and western Pacific sectors. In the former region, the equatorial outflow subsides over India, with relative drying compared to GLOB. The flow reverses over the western Pacific, where the equatorial subsidence is accompanied by ascent and upper-level divergence over the north-western Pacific. Notwithstanding the reduction of the GLOB biases in the equatorial region, the induced meridional vertical circulations in GLOB_A result in additional drying over India and wettening over the western subtropical Pacific, including south-eastern China, due to improved anticyclonic moisture transport from the equator (Fig. 2d).

Thus, GLOB_A further reduces the wind and precipitation biases in most of the oceanic areas (Figs. 2b and 2d ; e.g. the MC and the double ITCZ region), indicating the important role of near-surface processes there. Yet, the model adjustment in the circulation induces anomalous convective cells, particularly evident in the summer, which worsen its performance in the northern subtropics. GLOB_A better simulates the near-surface winds over India and China in both seasons, yet the precipitation only improves over China in the winter. One direct implication is that an improved simulation of the WPSH may not alleviate the wet summertime bias over China.

3.4 Effect of remote versus local nudging

Here, we analyse the ELSE and ASIA experiments (i.e., the atmospheric circulation is nudged outside and over Asia, respectively), to disentangle the relative contribution of regional and remote circulation biases in driving the model errors over Asia (Figs. 2e and 2h). Both experiments share overall similar precipitation and near-surface wind anomaly patterns to those of GLOB and GLOB_A, though there are some local differences as expected given the regional nature of the imposed relaxation term.

During the winter, compared to GLOB, ELSE features a decrease of precipitation over the equatorial MC area (Figs. 2a and 2e), resulting in a larger precipitation deficit than GLOB (Table 2). By contrast, ASIA is slightly wetter than GLOB over the same area suggesting circulation anomalies over Asia may play an important role in modulating the MC bias. This can also be inferred from the pattern of the anomalous 200-hPa divergent circulation (Fig. 3). The rainfall deficit over the MC is associated with a strong upper-level southward inflow coming from the East China Sea (Figs. 3a, 3e, and 3g), with compensating northward near-surface return flow (Figs. 2a, 2e, and 2g). This anomalous circulation cell is clearly recognizable in ELSE but is much weaker in GLOB and ASIA. Over India, ASIA further reduces the GLOB dry bias compared to observations, while ELSE induces a larger wet bias (Table 2). Similarly, the excess rainfall over central and eastern China in GLOB improves only with regional nudging, while it deteriorates when the local circulation is free to evolve. These results suggest a realistic representation of the local circulation to be more important than that over the surrounding regions for improving the model skill at simulating wintertime precipitation over the Indian subcontinent and China.

The summer dry bias over the Indian sector is smaller for the ASIA experiment than for ELSE (Table 2), indicating that the circulation over the Indian subcontinent is more crucial to alleviate the dry summertime bias. Excess precipitation over the equatorial Indian ocean also shows stronger reduction in ASIA than in ELSE (Table 2). Yet, prescribing the circulation either regionally or remotely generally results in much larger biases than with global nudging, indicating the key role of non-linear interactions between the two.

The anomalous meridional precipitation dipole over the western Pacific is larger and more longitudinally extensive in ASIA than in ELSE compared to observations, associated with a stronger anomalous cyclone bias in the former (Figs. 2f and 2h). Over central-eastern China, ELSE and ASIA, as with GLOB, reverse the sign of the CONT rainfall dry bias (Table 2), associated with an anomalous anticyclone over the East China Sea and related southerly wind anomalies along its western flank (Fig. S4). However, the magnitude of the wet bias is smaller in ELSE than in ASIA (Table 2). Nudging both local and remote circulation (GLOB) causes a wet bias of 1.0 mm/day, and all nudged experiments overestimate the magnitude of the bias in the control experiment. This suggests that nudging circulation over Asia causes a too-strong adjustment to precipitation that overcompensates for the original model bias. These results emphasize the key role of the model representation of the WPSH in modulating rainfall and circulation biases over the western Pacific and eastern China, consistently with previous studies (Gao et al., 2014; Wang et al., 2013). In turn, biases in the simulated circulation over Asia do have an influence, although secondary to those outside Asia, on location and magnitude of the WPSH (Figs. 3f and 3h).

3.5 The response of precipitation variability to nudging

Several studies have suggested cross-scale interactions may be fundamental in modulating the Asian monsoon annual cycle. For example, IAV of the seasonal mean monsoon rainfall is affected by the nature of ISV (e.g., Yoo et al. 2010), and a realistic representation of these relationship is key for improved seasonal monsoon simulations and predictions (e.g., Achuthavarier & Krishnamurthy, 2010; Fang et al., 2017). Summertime monsoon precipitation variability is closely linked to the occurrence of severe droughts and floods, which have considerable influence on agriculture, economy, and social well-being across Asia (Udmale et al., 2014; Zheng et al., 2006). Here, we evaluate model precipitation variability on two main time scales: IAV and ISV.

Large observed IAV occurs along the equatorial Indian Ocean and the western coast of India, over the northern BOB, and over the northwestern tropical Pacific (Fig. 5a; e.g., Ferranti et al., 1997), which corresponds to areas with large precipitation and warm SST in the seasonal mean (Fig. S2b). The spatial pattern of observed ISV has a close resemblance to that of IAV (Zhang et al., 2019), possibly due to the scale interactions and suggesting a common pattern of variability (Goswami & Mohan, 2001). Note that ISV has a magnitude about 2.5 times the amplitude of IAV (e.g., Achuthavarier & Krishnamurthy, 2010; Ferranti et al., 1997), with largest values over the South China Sea and the Philippine Sea (Fig. 5b). CONT generally captures the observed spatial structure of both IAV and ISV and their relative magnitude (Figs. 5c and 5d). A notable difference is the northward displacement of the maximum IAV over the northern subtropical Pacific.

The simulated amplitude of both IAV and ISV is considerably higher than observed in most regions, except over the south-equatorial MC, western half of India and the nearby northern Arabian Sea. The resulting quadrupole pattern of variability anomaly across the Indian-western Pacific sector resembles that of the seasonal mean bias (Figs. 5e and 5f). These patterns are consistent with previous findings, which show that precipitation-latent heat flux feedback acts to reduce the overestimated variability in AGCMs when coupled to ocean models (e.g., Fang et al., 2017; Wu & Kirtman, 2005).

Nudging above the boundary layer (Figs. 6a and 6b) improves the spatial structure of the simulated IAV and ISV over a large part of the domain, in particular over western India and the western subtropical Pacific. However, GLOB shows negligible improvements or even deterioration compared to CONT over the MC, the western equatorial Pacific and the SPCZ, similar to the corresponding changes in the seasonal mean. This suggests a stronger influence of the circulation on precipitation variability outside the deep tropics (Rasmusson and Arkin, 1993; Seager et al., 2005). Conversely, nudging tends to degrade the skill in simulated variability over the oceanic deep convective regions. The similarity in the IAV and ISV pattern changes suggests the presence of common controls, possibly stemming from the relationship between monsoon variability and the underlying seasonally persistent mode (e.g., Krishnamurthy and Shukla 2000).

Additional boundary layer nudging (GLOB_A) further improves the simulated IAV and ISV with respect to GLOB, with the largest improvements across the equatorial Indo-Pacific region (Figs. 6c and 6d). Thus, while model skill in simulating the subtropical variability increases with the extent of vertical nudging, nudging only above the boundary layer actually deteriorates the simulated near-equatorial variability. This emphasises the importance of correctly representing sub-daily coupled processes at the ocean-atmosphere interface for the successful simulation of rainfall in the strongly convective regions. Examination of the regional nudged experiments (Figs. 6e–6h) shows that both ASIA and ELSE have a very close resemblance to GLOB over the nudged domain (Asia and outside Asia, respectively), while they display differences over the free-running region (where they both show similar patterns to CONT). This suggests precipitation variability to be largely dominated by the local circulation.

3.6 The response of the El Niño-monsoon relationship and monsoon onset dates

Improvements in the simulated precipitation IAV and ISV may translate into a more skilful representation of the Asian monsoon link with the El Niño and of monsoon onset, respectively. El Niño is known to exert a strong influence on the Asian monsoon variability at interannual timescale (Lau and Nath 2000; Wang et al. 2000, 2013), while the onset of the rainy season is related to the active and break spells of the monsoon modulated by intraseasonal monsoon oscillations (e.g., Karmakar and Misra 2019). A better representation of these features is crucial for seasonal monsoon forecasts (Achuthavarier et al., 2012; Wu et al., 2009), as well as the establishment of low-level wind reversal and rainfall season (Qi et al., 2009; Wang et al., 2018).

During El Niño events, rainfall decreases over the MC (Fig. 7a), resulting from the eastward displacement of the rising branch of the Walker circulation and corresponding convection (Lau and Nath, 2000). To its northwest, an anomalous low-tropospheric anticyclonic circulation develops over the north-equatorial Indian Ocean, consistent with a Gill-type response to the suppressed diabatic heating over Indonesia. Divergent easterly anomalies and subsidence over the south-equatorial Indian Ocean lead to northerlies over India and general drier conditions and thus to a weaker Indian monsoon (Ramu et al., 2018), while westerly anomalies over the equatorial western Pacific weaken the WPSH, leading to a south-wet-north-dry rainfall anomalous pattern over eastern China and a dipolar precipitation anomaly over the equatorial pacific (e.g., Wang et al. 2020). The positive rainfall anomaly over the central India core monsoon area is also noteworthy as it has recently been suggested to be associated with multi-decadal variations in the ENSO-monsoon relationship (Srivastava et al., 2019) , albeit largely muted in the long-term record (Wang et al., 2020).

In CONT, the ENSO convection dipole over the MC and the western Pacific is more intense and shifted north-eastward compared to observations (Fig. 7b). This results in the displacement of the anticyclonic anomaly from the north-equatorial Indian ocean to central India, leading to widespread drying over the Indian subcontinent and the Bay of Bengal. Additionally, the cyclonic anomaly over the western subtropical Pacific intensifies and shifts northward, leading to strong northerlies and a precipitation deficit across eastern China. GLOB significantly improves the precipitation and low-tropospheric circulation anomalies over the entire Indo-Pacific sector (Fig. 7c). The observed MC equatorial precipitation and circulation anomalies are reproduced well, which in turn result in a realistic spatial pattern of the ENSO teleconnection to the north, including the rainfall meridional dipoles over northern India and eastern China.

Compared to GLOB, the major improvements in GLOB_A are seen over the tropics such as the better representation of the easterlies over the western MC and the equatorial Indian Ocean sector and of the westerlies over the western equatorial Pacific (Fig. S8d). The resulting more organised anticyclonic flow over the Indian sector further reduces dry biases over India (Fig. 7d). Inspection of the regionally-nudged experiments in comparison to GLOB and observations shows that, while ASIA displays a too strong and northeastward displaced convective dipole over the western equatorial Pacific, similar to CONT, it better simulates rainfall and the westerlies circulation anomalies over Indochina and the MC, which are conversely too large and strong in ELSE, resulting in more realistic rainfall patterns over India and China (Figs. 7e and 7f). This further emphasises the important role of regional circulation over Asia, and particularly over the MC, in realising the ENSO teleconnections to India and China.

The monsoon onset, heralding the transition to the rainy season, is critical for agriculture and economy across Asia; yet its prediction represents a major challenge (Martin et al., 2019; Wang et al., 2009). Observations show the monsoon establishment from early to mid-May (pentads 25–29) in a northeastward oriented band extending from southern Indonesia to Japan, representing the Mei-Yu front (Fig. 8a). The onset of the monsoon rainy season occurs progressively later northwestward from the monsoon oceans toward inland areas, with a migration from the BOB (pentad 24) toward northwest India (pentad 37). Note also the delayed progression over the subtropical western Pacific.

The most striking feature of the bias in the onset pattern simulated by CONT is the large delay over India and the BOB (exceeding 8 pentads; see Fig. 8b), which is not surprising given the large dry bias over the region. The onset is also delayed, although to a lesser extent (~3–4 pentads), over a southwest to northeast band extending from Indochina to the south of Japan across southeastern China. This bias is associated with the model difficulty in representing the seasonal mean northward extent of the Mei-Yu, which conversely tends to stagnate to the south (Wilcox et al., 2015). In turn, this leads to an earlier onset over the western Pacific. This contrasts with the earlier onset of the monsoon rains over central and northern China, likely reflecting the contribution of local convective activity rather than the northwestward migration of the front.

GLOB significantly improves the simulated onset date over most the domain (Fig. 8c), including a critical advancement of the monsoon by 2–4 pentads over central and western India. However, monsoon rains are further delayed in GLOB over the eastern equatorial Indian Ocean and the South China Sea, and arrive too early (by an additional 1–2 pentads) over central and northern China. The changes of onset date caused by nudging are generally consistent with seasonal mean responses except over the South China Sea, suggesting an opposite effect of global nudging on IAV and ISV there.

GLOB_A leads to minor changes relative to GLOB (Fig. 8d). ELSE and ASIA produce opposite results over the Indian sector. While ELSE has an earlier and more realistic onset date over the eastern equatorial Indian Ocean and the BOB than ASIA, the northwestern march of the onset date across central and northern India is better captured by ASIA than by ELSE. This suggests the late-spring migration of the monsoon across the Indian Ocean and the BOB is related to the large-scale northward shift of rainfall from the western equatorial Pacific following the movement of the warm SSTs. Conversely, regional circulation is key to the further progression of the monsoon inland-ward across India, possibly associated with local land-atmosphere interactions (Bollasina and Ming, 2013b). Monsoon withdrawal date and monsoon season length (defined following Wang & Ho, 2002) display similar response patterns to nudging to those of monsoon onset (not shown).

4 Discussion and Conclusions

Air temperature is allowed to evolve freely as only winds are nudged in the above experiments. Fig. S9 shows that nudging both winds and temperature over the whole atmospheric column reduces the summer double ITCZ bias in GLOB_A as the latent heat released from convection is further constrained by temperature nudging. However, the dry bias over India becomes even larger in summer compared to that in GLOB_A, implying that temperature nudging can potentially generate new biases. Besides, humidity nudging may also be important for some regions although the anomalies of dynamical term broadly dominate the biases in moisture flux convergence and precipitation in nudged experiments (Figs. S6 and S7). Sun et al. (2019) found that humidity nudging dramatically improves the correlation of tropical precipitation with observations but further increases biases in the long-term simulated cloud and precipitation in the Energy Exascale Earth System Model Atmosphere Model Version 1. Note the nudging effect may be model dependent. Indeed, Wehrli et al. (2018) suggest that the temperature and precipitation biases are thermodynamically driven by local processes including land-atmosphere interactions and atmospheric parameterizations as most of the biases remains after constraining the large-scale circulation. Thus, the robustness of the findings needs to be evaluated using other climate models.

This study investigates the impact of atmospheric circulation biases on the simulation of the Asian monsoon seasonal mean climate and variability. We nudge model winds toward the ERA-I reanalysis and quantify the effects on model biases. Additionally, we separate the contribution of circulation errors over Asia and those outside Asia to monsoon precipitation biases, and provide insights into the associated mechanism underpinning the precipitation changes. Despite the remaining errors in nudged simulations, our study suggests that dynamical nudging serves as a useful tool to disentangle the contribution of regional and remote circulation in generating monsoon biases.

Nudging the circulation globally (GLOB) substantially reduces seasonal precipitation biases. Key features include a decrease of the dry bias over the Maritime Continent (MC) in winter and a quadrupole pattern of precipitation changes opposite to the bias in summer, associated with an enhanced western Pacific subtropical high (WPSH). The resulting low-level circulation changes serve to alleviate precipitation biases over India and China, showing teleconnections from MC and WPSH to the Asian winter and summer monsoon, respectively (Robertson et al., 2011; Wang et al., 2013). However, the double-ITCZ problem in summer is amplified because nudging cannot constrain sub-grid convection. Additional nudging in the boundary layer (GLOB_A) further reduces the dry bias over the MC in winter, suggesting the importance of simulating boundary layer circulation associated with an improved representation of complex terrain effects and the land-sea breeze circulation (Im & Eltahir, 2018). Constraining the circulation only over or outside Asia (i.e., the ASIA or ELSE experiments) reveals that precipitation biases are mainly driven by local circulation errors over eastern China and India. An exception is the summer precipitation bias over eastern China which is more controlled by WPSH anomalies.

The similarity of spatial patterns of interannual variability (IAV) and intraseasonal variability (ISV) in both observations and CONT suggests their cross-scale interactions (Yoo et al., 2010). Both GLOB and GLOB_A reduce the generally overestimated magnitude of the IAV and ISV in CONT over the subtropics, which translates a more skillful simulation of the Asian monsoon linkage with El Niño and the monsoon onset, respectively. The ASIA and ELSE experiments resemble GLOB over the nudged domain and CONT over the free-running region in both variability and El Niño teleconnections to India and China. This suggests a dominant role of local circulation anomalies. Over the Indian sector, ELSE better simulates onset date over the equatorial Indian Ocean and the BOB, while ASIA has a more realistic onset over central and northern India.

The results in this study help us identify processes that cause biases and understand the interplay between the Asian monsoon and the large-scale circulation. Understanding these interactions and the associated mechanisms is critical to improve the simulation of the Asian monsoon and its responses to anthropogenic forcing for better risk management and adaptation planning in this densely populated region.

Data Availability Statement

The GPCP and CMAP observational datasets are obtained from https://www.esrl.noaa.gov/psd/data/gridded/data.gpcp.html and https://psl.noaa.gov/data/gridded/data.cmap.html, respectively. The ERA-I reanalysis is provided by the European Centre for Medium-Range Weather Forecasts (https://www.ecmwf.int/en/forecasts/datasets/reanalysis-datasets/era-interim). The model outputs in reproducing this work are archived on zenodo (http://doi.org/10.5281/zenodo.4895856).

Acknowledgements

The authors would like to thank three anonymous reviewers for their constructive and insightful comments. ZL, MAB, LJW, and LAR were supported by the UK-China Research and Innovation Partnership Fund through the Met Office Climate Science for Service Partnership (CSSP) China as part of the Newton Fund. LAR acknowledge funding from NERC under the A-CURE grant (NE/P013406/1). We thank Nicolas Freychet for setting up the model, and Sean Milton and Ben Johnson for helpful discussions. We acknowledge the use of ARCHER, the UK HPC, and JASMIN to conduct the model simulations.

References

Achuthavarier, D., Krishnamurthy, V., Kirtman, B. P., & Huang, B. (2012). Role of the Indian Ocean in the ENSO-Indian summer monsoon teleconnection in the NCEP climate forecast system. *Journal of Climate*. https://doi.org/10.1175/JCLI-D-11-00111.1

Achuthavarier, D., & Krishnamurthy, V. (2010). Relation between intraseasonal and interannual variability of the South Asian monsoon in the National Centers for Environmental Predictions forecast systems. *Journal of Geophysical Research Atmospheres*. https://doi.org/10.1029/2009JD012865

Adler, R. F., Huffman, G. J., Chang, A., Ferraro, R., Xie, P. P., Janowiak, J., … Nelkin, E. (2003). The version-2 global precipitation climatology project (GPCP) monthly precipitation analysis (1979-present). *Journal of Hydrometeorology*. https://doi.org/10.1175/1525-7541(2003)004<1147:TVGPCP>2.0.CO;2

Bollasina, M. A., & Ming, Y. (2013a). The general circulation model precipitation bias over the southwestern equatorial Indian Ocean and its implications for simulating the South Asian monsoon. *Climate Dynamics*. https://doi.org/10.1007/s00382-012-1347-7

Bollasina, M. A., & Ming, Y. (2013b). The role of land-surface processes in modulating the Indian monsoon annual cycle. *Climate Dynamics*. https://doi.org/10.1007/s00382-012-

1634-3

Bollasina, M., & Nigam, S. (2009). Indian Ocean SST, evaporation, and precipitation during the South Asian summer monsoon in IPCC-AR4 coupled simulations. *Climate Dynamics*. https://doi.org/10.1007/s00382-008-0477-4

Chen, W., Hans-F., G., & Huang, R. (2000). The Interannual Variability of East Asian Winter Monsoon and Its Relation to the Summer Monsoon. *Advances in Atmospheric Sciences*.

Christidis, N., Stott, P. A., Scaife, A. A., Arribas, A., Jones, G. S., Copsey, D., … Tennant, W. J. (2013). A new HADGEM3-a-based system for attribution of weather- and climate-related extreme events. *Journal of Climate*. https://doi.org/10.1175/JCLI-D-12-00169.1

Dee, D. P., Uppala, S. M., Simmons, A. J., Berrisford, P., Poli, P., Kobayashi, S., … Vitart, F. (2011). The ERA-Interim reanalysis: Configuration and performance of the data assimilation system. *Quarterly Journal of the Royal Meteorological Society*. https://doi.org/10.1002/qj.828

Deser, C., Phillips, A., Bourdette, V., & Teng, H. (2012). Uncertainty in climate change projections: The role of internal variability. *Climate Dynamics*. https://doi.org/10.1007/s00382-010-0977-x

Eden, J. M., Widmann, M., Grawe, D., & Rast, S. (2012). Skill, correction, and downscaling of GCM-simulated precipitation. *Journal of Climate*. https://doi.org/10.1175/JCLI-D-11-00254.1

Fang, Y., Wu, P., Mizielinski, M. S., Roberts, M. J., Li, B., Xin, X., & Liu, X. (2017). Monsoon intra-seasonal variability in a high-resolution version of Met Office Global Coupled model. *Tellus, Series A: Dynamic Meteorology and Oceanography*. https://doi.org/10.1080/16000870.2017.1354661

Feichter, J., & Lohmann, U. (1999). Can a relaxation technique be used to validate clouds and sulphur species in a GCM? *Quarterly Journal of the Royal Meteorological Society*. https://doi.org/10.1002/qj.1999.49712555609

Ferranti, L., Slingo, J. M., Palmer, T. N., & Hoskins, B. J. (1997). Relations between interannual and intraseasonal monsoon variability as diagnosed from AMIP integrations. *Quarterly Journal of the Royal Meteorological Society*. https://doi.org/10.1256/smsqj.54109

Gao, H., Jiang, W., & Li, W. (2014). Changed relationships between the east asian summer monsoon circulations and the summer rainfall in eastern china. *Journal of Meteorological Research*. https://doi.org/10.1007/s13351-014-4327-5

Ghan, S., Laulainen, N., Easter, R., Wagener, R., Nemesure, S., Chapman, E., … Leung, R. (2001). Evaluation of aerosol direct radiative forcing in MIRAGE. *Journal of Geophysical Research Atmospheres*. https://doi.org/10.1029/2000JD900502

Goswami, B. N., & Ajaya Mohan, R. S. (2001). Intraseasonal oscillations and interannual variability of the Indian summer monsoon. *Journal of Climate*. https://doi.org/10.1175/1520-0442(2001)014<1180:IOAIVO>2.0.CO;2

Greatbatch, R. J., Sun, X., & Yang, X. Q. (2013). Impact of variability in the Indian summer monsoon on the East Asian summer monsoon. *Atmospheric Science Letters*. https://doi.org/10.1002/asl2.408

He, C., & Zhou, T. (2014). The two interannual variability modes of the Western North Pacific Subtropical High simulated by 28 CMIP5–AMIP models. *Climate Dynamics*. https://doi.org/10.1007/s00382-014-2068-x

Hoesly, R. M., Smith, S. J., Feng, L., Klimont, Z., Janssens-Maenhout, G., Pitkanen, T., … Zhang, Q. (2018). Historical (1750-2014) anthropogenic emissions of reactive gases and aerosols from the Community Emissions Data System (CEDS). *Geoscientific Model Development*. https://doi.org/10.5194/gmd-11-369-2018

Im, E. S., & Eltahir, E. A. B. (2018). Simulation of the diurnal variation of rainfall over the western Maritime Continent using a regional climate model. *Climate Dynamics*. https://doi.org/10.1007/s00382-017-3907-3

Jiang, X., Li, Y., Yang, S., Yang, K., & Chen, J. (2016). Interannual variation of summer atmospheric heat source over the Tibetan Plateau and the role of convection around the Western Maritime Continent. *Journal of Climate*. https://doi.org/10.1175/JCLI-D-15-0181.1

Johnson, B. T., Haywood, J. M., & Hawcroft, M. K. (2019). Are Changes in Atmospheric Circulation Important for Black Carbon Aerosol Impacts on Clouds, Precipitation, and Radiation? *Journal of Geophysical Research: Atmospheres*. https://doi.org/10.1029/2019jd030568

Kang, I. S., Jin, K., Wang, B., Lau, K. M., Shukla, J., Krishnamurthy, V., … Liu, Y. (2002). Intercomparison of the climatological variations of Asian summer monsoon precipitation simulated by 10 GCMs. *Climate Dynamics*. https://doi.org/10.1007/s00382-002-0245-9

Karmakar, N., & Misra, V. (2019). The Relation of Intraseasonal Variations With Local Onset and Demise of the Indian Summer Monsoon. *Journal of Geophysical Research: Atmospheres*. https://doi.org/10.1029/2018JD029642

Kooperman, G. J., Pritchard, M. S., Ghan, S. J., Wang, M., Somerville, R. C. J., & Russell, L. M. (2012). Constraining the influence of natural variability to improve estimates of global aerosol indirect effects in a nudged version of the Community Atmosphere Model 5. *Journal of Geophysical Research Atmospheres*. https://doi.org/10.1029/2012JD018588

Krishnamurthy, V., & Shukla, J. (2000). Intraseasonal and interannual variability of rainfall over India. *Journal of Climate*. https://doi.org/10.1175/1520-0442(2000)013<0001:IAIVOR>2.0.CO;2

Kumar, K. K., Hoerling, M., & Rajagopalan, B. (2005). Advancing dynamical prediction of Indian monsoon rainfall. *Geophysical Research Letters*. https://doi.org/10.1029/2004GL021979

Lau, N. C., & Nath, M. J. (2000). Impact of ENSO on the variability of the Asian-Australian Monsoons as simulated in GCM experiments. *Journal of Climate*. https://doi.org/10.1175/1520-0442(2000)013<4287:IOEOTV>2.0.CO;2

Li, Y., & Yang, S. (2010). A dynamical index for the East Asian winter monsoon. *Journal of Climate*. https://doi.org/10.1175/2010JCLI3375.1

Lin, G., Wan, H., Zhang, K., Qian, Y., & Ghan, S. J. (2016). Can nudging be used to quantify model sensitivities in precipitation and cloud forcing? *Journal of Advances in Modeling*

Earth Systems. https://doi.org/10.1002/2016MS000659

Lin, H. (2009). Global extratropical response to diabatic heating variability of the Asian summer monsoon. *Journal of the Atmospheric Sciences*. https://doi.org/10.1175/2009JAS3008.1

Liu, Y., Li, W., Zuo, J., & Hu, Z. Z. (2014). Simulation and projection of the western pacific subtropical high in CMIP5 models. *Journal of Meteorological Research*. https://doi.org/10.1007/s13351-014-3151-2

Lohmann, U., & Hoose, C. (2009). Sensitivity studies of different aerosol indirect effects in mixed-phase clouds. *Atmospheric Chemistry and Physics*. https://doi.org/10.5194/acp-9-8917-2009

Martin, G. M., Chevuturi, A., Comer, R. E., Dunstone, N. J., Scaife, A. A., & Zhang, D. (2019). Predictability of South China Sea Summer Monsoon Onset. *Advances in Atmospheric Sciences*. https://doi.org/10.1007/s00376-018-8100-z

Mulcahy, J. P., Jones, C., Sellar, A., Johnson, B., Boutle, I. A., Jones, A., … McCoy, D. T. (2018). Improved Aerosol Processes and Effective Radiative Forcing in HadGEM3 and UKESM1. *Journal of Advances in Modeling Earth Systems*. https://doi.org/10.1029/2018MS001464

Neale, R., & Slingo, J. (2003). The Maritime Continent and its role in the global climate: A GCM study. *Journal of Climate*. https://doi.org/10.1175/1520-0442(2003)016<0834:TMCAIR>2.0.CO;2

Nigam, S., & Chan, S. C. (2009). On the summertime strengthening of the Northern Hemisphere Pacific sea level pressure anticyclone. *Journal of Climate*. https://doi.org/10.1175/2008JCLI2322.1

Prodhomme, C., Terray, P., Masson, S., Izumo, T., Tozuka, T., & Yamagata, T. (2014). Impacts of Indian Ocean SST biases on the Indian Monsoon: As simulated in a global coupled model. *Climate Dynamics*. https://doi.org/10.1007/s00382-013-1671-6

Qi, Y., Zhang, R., Li, T., & Wen, M. (2009). Impacts of intraseasonal oscillation on the onset and interannual variation of the Indian summer monsoon. *Chinese Science Bulletin*. https://doi.org/10.1007/s11434-008-0441-z

Ramesh, K. V., & Goswami, P. (2014). Assessing reliability of regional climate projections: The case of Indian monsoon. *Scientific Reports*. https://doi.org/10.1038/srep04071

Ramu, D. A., Chowdary, J. S., Ramakrishna, S. S. V. S., & Kumar, O. S. R. U. B. (2018). Diversity in the representation of large-scale circulation associated with ENSO-Indian summer monsoon teleconnections in CMIP5 models. *Theoretical and Applied Climatology*. https://doi.org/10.1007/s00704-017-2092-y

Rasmusson, E. M., & Arkin, P. A. (1993). A global view of large-scale precipitation variability. *Journal of Climate*. https://doi.org/10.1175/1520-0442(1993)006<1495:AGVOLS>2.0.CO;2

Regayre, L. A., Pringle, K. J., Booth, B. B. B., Lee, L. A., Mann, G. W., Browse, J., … Carslaw, K. S. (2014). Uncertainty in the magnitude of aerosol-cloud radiative forcing over recent decades. *Geophysical Research Letters*. https://doi.org/10.1002/2014GL062029

Regayre, Leighton A., Johnson, J. S., Yoshioka, M., Pringle, K. J., Sexton, D. M. H., Booth, B. B. B., … Carslaw, K. S. (2018). Aerosol and physical atmosphere model parameters are both important sources of uncertainty in aerosol ERF. *Atmospheric Chemistry and Physics*. https://doi.org/10.5194/acp-18-9975-2018

Robertson, A. W., MORON, V., QIAN, J.-H., CHANG, C.-P., TANGANG, F., ALDRIAN, E., … LIEW, J. (2011). The maritime continent monsoon. https://doi.org/10.1142/9789814343411_0006

Rodríguez, J. M., Milton, S. F., & Marzin, C. (2017). The East Asian Atmospheric Water Cycle and Monsoon Circulation in the Met Office Unified Model. *Journal of Geophysical Research: Atmospheres*. https://doi.org/10.1002/2016JD025460

Rodríguez, J. M., & Milton, S. F. (2019). East Asian Summer Atmospheric Moisture Transport and Its Response to Interannual Variability of the West Pacific Subtropical High: An Evaluation of the Met Office Unified Model. *Atmosphere*. https://doi.org/10.3390/atmos10080457

Rodwell, M. J., & Hoskins, B. J. (1996). Monsoons and the dynamics of deserts. *Quarterly Journal of the Royal Meteorological Society*. https://doi.org/10.1256/smsqj.53407

Russell, D. R. (2006). Measurement Procedure for Application at Regional and Teleseismic Distances , Part I : Theory. *Bulletin of the Seismological Society of America*. https://doi.org/10.1785/0120050055

Sardeshmukh, P. D., & Hoskins, B. J. (1988). The generation of global rotational flow by steady idealized tropical divergence. *Journal of the Atmospheric Sciences*. https://doi.org/10.1175/1520-0469(1988)045<1228:TGOGRF>2.0.CO;2

Seager, Rich, Harnik, N., Robinson, W. A., Kushnir, Y., Ting, M., Huang, H. P., & Velez, J. (2005). Mechanisms of ENSO-forcing of hemispherically symmetric precipitation variability. *Quarterly Journal of the Royal Meteorological Society*. https://doi.org/10.1256/qj.04.96

Seager, Richard, Naik, N., & Vecchi, G. A. (2010). Thermodynamic and dynamic mechanisms for large-scale changes in the hydrological cycle in response to global warming. *Journal of Climate*. https://doi.org/10.1175/2010JCLI3655.1

Shepherd, T. G. (2014). Atmospheric circulation as a source of uncertainty in climate change projections. *Nature Geoscience*. https://doi.org/10.1038/NGEO2253

Song, F., & Zhou, T. (2014a). Interannual variability of East Asian summer monsoon simulated by CMIP3 and CMIP5 AGCMs: Skill dependence on Indian Ocean-western pacific anticyclone teleconnection. *Journal of Climate*. https://doi.org/10.1175/JCLI-D-13-00248.1

Song, F., & Zhou, T. (2014b). The climatology and interannual variability of east Asian summer monsoon in CMIP5 coupled models: Does air-sea coupling improve the simulations? *Journal of Climate*. https://doi.org/10.1175/JCLI-D-14-00396.1

Sperber, K. R., Annamalai, H., Kang, I. S., Kitoh, A., Moise, A., Turner, A., … Zhou, T. (2013). The Asian summer monsoon: An intercomparison of CMIP5 vs. CMIP3 simulations of the late 20th century. *Climate Dynamics*. https://doi.org/10.1007/s00382-012-1607-6

Srivastava, G., Chakraborty, A., & Nanjundiah, R. S. (2019). Multidecadal see-saw of the impact of ENSO on Indian and West African summer monsoon rainfall. *Climate Dynamics*. https://doi.org/10.1007/s00382-018-4535-2

Sun, J., Zhang, K., Wan, H., Ma, P. L., Tang, Q., & Zhang, S. (2019). Impact of Nudging Strategy on the Climate Representativeness and Hindcast Skill of Constrained EAMv1 Simulations. *Journal of Advances in Modeling Earth Systems*. https://doi.org/10.1029/2019MS001831

Telford, P. J., Braesicke, P., Morgenstern, O., & Pyle, J. A. (2008). Technical note: Description and assessment of a nudged version of the new dynamics Unified Model. *Atmospheric Chemistry and Physics*. https://doi.org/10.5194/acp-8-1701-2008

Toh, Y. Y., Turner, A. G., Johnson, S. J., & Holloway, C. E. (2018). Maritime Continent seasonal climate biases in AMIP experiments of the CMIP5 multimodel ensemble. *Climate Dynamics*. https://doi.org/10.1007/s00382-017-3641-x

Udmale, P., Ichikawa, Y., Manandhar, S., Ishidaira, H., & Kiem, A. S. (2014). Farmers' perception of drought impacts, local adaptation and administrative mitigation measures in Maharashtra State, India. *International Journal of Disaster Risk Reduction*. https://doi.org/10.1016/j.ijdrr.2014.09.011

Walters, D., Baran, A. J., Boutle, I., Brooks, M., Earnshaw, P., Edwards, J., … Zerroukat, M. (2019). The Met Office Unified Model Global Atmosphere 7.0/7.1 and JULES Global Land 7.0 configurations. *Geoscientific Model Development*, *12*(5), 1909–1963. https://doi.org/10.5194/gmd-12-1909-2019

Wang, B., Wu, R., & Fu, X. (2000). Pacific-East Asian teleconnection: How does ENSO affect East Asian climate? *Journal of Climate*. https://doi.org/10.1175/1520-0442(2000)013<1517:PEATHD>2.0.CO;2

Wang, B., & Ho, L. (2002). Rainy season of the Asian-Pacific summer monsson. *Journal of Climate*. https://doi.org/10.1175/1520-0442(2002)015<0386:RSOTAP>2.0.CO;2

Wang, B., Ding, Q., & Joseph, P. V. (2009). Objective definition of the Indian summer monsoon onset. *Journal of Climate*. https://doi.org/10.1175/2008JCLI2675.1

Wang, B., Xiang, B., & Lee, J. Y. (2013). Subtropical High predictability establishes a promising way for monsoon and tropical storm predictions. *Proceedings of the National Academy of Sciences of the United States of America*. https://doi.org/10.1073/pnas.1214626110

Wang, B., Luo, X., & Liu, J. (2020). How Robust is the Asian Precipitation–ENSO Relationship during the Industrial Warming Period (1901–2017)? *Journal of Climate*. https://doi.org/10.1175/jcli-d-19-0630.1

Wang, H., Liu, F., Wang, B., & Li, T. (2018). Effects of intraseasonal oscillation on South China Sea summer monsoon onset. *Climate Dynamics*. https://doi.org/10.1007/s00382-017-4027-9

Wehrli, K., Guillod, B. P., Hauser, M., Leclair, M., & Seneviratne, S. I. (2018). Assessing the Dynamic Versus Thermodynamic Origin of Climate Model Biases. *Geophysical Research Letters*. https://doi.org/10.1029/2018GL079220

Wei, K., Xu, T., Du, Z., Gong, H., & Xie, B. (2014). How well do the current state-of-the-art CMIP5 models characterise the climatology of the East Asian winter monsoon? *Climate Dynamics*. https://doi.org/10.1007/s00382-013-1929-z

Wilcox, L. J., Dong, B., Sutton, R. T., & Highwood, E. J. (2015). The 2014 hot, dry summer in northeast Asia. *Bulletin of the American Meteorological Society*. https://doi.org/10.1175/BAMS-D-15-00123.1

Williams, K. D., Copsey, D., Blockley, E. W., Bodas-Salcedo, A., Calvert, D., Comer, R., … Xavier, P. K. (2018). The Met Office Global Coupled Model 3.0 and 3.1 (GC3.0 and GC3.1) Configurations. *Journal of Advances in Modeling Earth Systems*. https://doi.org/10.1002/2017MS001115

Wu, R., & Kirtman, B. P. (2005). Roles of Indian and Pacific Ocean air-sea coupling in tropical atmospheric variability. *Climate Dynamics*. https://doi.org/10.1007/s00382-005-0003-x

Wu, Z., Wang, B., Li, J., & Jin, F. F. (2009). An empirical seasonal prediction model of the east Asian summer monsoon using ENSO and NAO. *Journal of Geophysical Research Atmospheres*. https://doi.org/10.1029/2009JD011733

Xie, P., & Arkin, P. A. (1997). Global Precipitation: A 17-Year Monthly Analysis Based on Gauge Observations, Satellite Estimates, and Numerical Model Outputs. *Bulletin of the American Meteorological Society*. https://doi.org/10.1175/1520-0477(1997)078<2539:GPAYMA>2.0.CO;2

Yang, B., Zhang, Y., Qian, Y., Song, F., Leung, L. R., Wu, P., … Huang, A. (2019). Better monsoon precipitation in coupled climate models due to bias compensation. *Npj Climate and Atmospheric Science*. https://doi.org/10.1038/s41612-019-0100-x

Yoo, J. H., Robertson, A. W., & Kang, I. S. (2010). Analysis of intraseasonal and interannual variability of the Asian summer monsoon using a hidden Markov model. *Journal of Climate*. https://doi.org/10.1175/2010JCLI3473.1

Zhang, J., Wang, H., & Liu, F. (2019). Inter-annual variability of boreal summer intra-Seasonal oscillation propagation from the Indian Ocean to the Western Pacific. *Atmosphere*. https://doi.org/10.3390/atmos10100596

Zhang, K., Wan, H., Liu, X., Ghan, S. J., Kooperman, G. J., Ma, P. L., … Lohmann, U. (2014). Technical note: On the use of nudging for aerosol-climate model intercomparison studies. *Atmospheric Chemistry and Physics*. https://doi.org/10.5194/acp-14-8631-2014

Zheng, J., Wang, W. C., Ge, Q., Man, Z., & Zhang, P. (2006). Precipitation variability and extreme events in eastern China during the past 1500 years. *Terrestrial, Atmospheric and Oceanic Sciences*. https://doi.org/10.3319/TAO.2006.17.3.579(A)

Zhou, T., Turner, A. G., Kinter, J. L., Wang, B., Qian, Y., Chen, X., … He, B. (2016). GMMIP (v1.0) contribution to CMIP6: Global Monsoons Model Inter-comparison Project. *Geoscientific Model Development*. https://doi.org/10.5194/gmd-9-3589-2016

Zhou, T., Wu, B., & Wang, B. (2009). How well do atmospheric general circulation models capture the leading modes of the interannual variability of the Asian-Australian monsoon? *Journal of Climate*. https://doi.org/10.1175/2008JCLI2245.1

Zhou, Z. Q., Xie, S. P., Zhang, G. J., & Zhou, W. (2018). Evaluating AMIP skill in simulating interannual variability over the Indo-western Pacific. *Journal of Climate*. https://doi.org/10.1175/JCLI-D-17-0123.1

Zou, L. (2020). Does regional air–sea coupling improve the simulation of the summer monsoon over the western North Pacific in the WRF4 model? *Atmospheric and Oceanic Science Letters*. https://doi.org/10.1080/16742834.2020.1819755

Figures and Tables

Table 1. Model simulations. The model layer 12 in hybrid-height vertical coordinate is treated as planetary boundary layer (PBL) height, which is around 850hPa in CONT. The location of Asia is represented by the purple box in Fig. 1a.

Experiment	Description
CONT	Free run without nudging applied
GLOB	Global horizontal wind nudging applied above PBL
GLOB_A	Global wind nudging applied over the whole atmospheric column
ELSE	Wind nudging above PBL applied outside Asia
ASIA	Wind nudging above PBL applied over Asia

*Table 2. Area-mean precipitation biases (unit: mm/day) over key regions in relative to observations. The numbers in the parenthesis represent the absolute percentage biases with respect to observational values. Abbreviations: MC, Maritime Continent; EC, eastern China; SPCZ, the South Pacific Convergence Zone; EIO: the equatorial Indian Ocean; NSCS: northern South China Sea, WPSH: the Western Pacific Subtropical High. Corresponding region boundaries for computing the area averages are denoted by rectangles in Fig. S3. Note locations of the regions may vary in summer and winter depending on where relatively strong nudging effects are found. * indicates that the area mean is computed over land grid points only.*

			Winter			
	MC	India*	EC*	SPCZ	EIO	NSCS
CONT	–3.1 (36%)	0.60 (157%)	1.0 (70%)	4.3 (49%)	1.6 (21%)	0.98 (54%)
GLOB	–2.4 (29%)	–0.02 (5%)	0.5 (38%)	1.5 (17%)	4.2 (55%)	0.53 (29%)
GLOB_A	–0.4 (5%)	–0.16 (42%)	0.1 (7%)	1.5 (17%)	3.7 (50%)	0.36 (20%)
ELSE	–2.7 (32%)	0.21 (55%)	0.9 (65%)	1.5 (18%)	4.1 (55%)	0.56 (31%)
ASIA	–2.1 (25%)	0.01 (3%)	0.4 (31%)	3.8 (43%)	2.5 (33%)	0.51 (28%)
			Summer			
	MC	India*	EC*	SPCZ	EIO	WPSH
CONT	–1.8 (38%)	–4.3 (57%)	–0.60 (10%)	4.2 (53%)	2.1 (36%)	5.8 (75%)
GLOB	–0.4 (9%)	–1.0 (14%)	1.0 (16%)	13.5 (169%)	1.8 (31%)	0.2 (2%)
GLOB_A	0.2 (4%)	–1.4 (19%)	1.0 (16%)	11.2 (141%)	1.9 (33%)	1.6 (21%)
ELSE	–0.9 (19%)	–2.4 (33%)	0.9 (15%)	13.0 (163%)	2.6 (45%)	1.1 (14%)
ASIA	–2.2 (47%)	–1.7 (23%)	1.3 (21%)	5.4 (68%)	1.8 (31%)	2.7 (34%)

Fig. 1. Bias in the control simulation measured as differences in precipitation (mm/day) and 925-hPa wind (m/s) with respect to the mean of GPCP and CMAP satellite product and ERA-I reanalysis, respectively, in (a) winter and (b) summer. (c, d) Same as (a, b) but for vertically-integrated stationary moisture flux convergence (MFC; mm/day) and moisture flux (MF; kg/m/s). (e, f) Same as (a, b) but for 200-hPa divergence (10^6/s) and divergent wind (m/s). Contours represent climatological ERA-I sea surface temperature (°C). Black dots indicate differences at the 90% significance level according to the Kolmogorov-Smirnov test. The purple box denotes the Asia region (10°–45°N, 60°–125°E).

Fig. 2. Biases in precipitation (mm/day) and 925-hPa wind (m/s) between GLOB and observations in (a) winter and (b) summer. (c, d), (e, f), and (g, h) Same as (a, b) but for GLOB_A, ELSE and ASIA simulations, respectively.

Fig. 3. Same as Fig. 2 but for 200-hPa divergence (10^6/s) and divergent wind (m/s).

Fig. 4. Differences in precipitation and 925-hPa wind between GLOB_A and GLOB in (a) winter and (b) summer. (c, d) Same as (a, b) but for 200-hPa divergence (10^6/s) and divergent wind (m/s).

Fig. 5. The summer climatology of precipitation (a) interannual variability (mm/day) and (b) intraseasonal variability (mm/day) measured as the average of GPCP and CMAP pentad precipitation variability. (c, d) Same as (a, b) but for CONT. Bias in the control simulation measured as the differences in summer precipitation (e) interannual variability and (f) intraseasonal variability in relative to observations.

Fig. 6. Bias in the GLOB measured as the differences in summer precipitation (a) interannual variability and (b) intraseasonal variability in relative to observations. (c, d), (e, f), and (g, h) Same as (a, b) but for GLOB_A, ELSE and ASIA simulations, respectively.

Fig. 7. Simultaneous regression coefficients of summer precipitation and 925-hPa wind onto Niño3.4 index in (a) observations, (b) CONT, (c) GLOB, (d) GLOB_A, (e) ELSE, and (f) ASIA. Black dots indicate the regression coefficients at the 90% significance level according to the Student's t *test.*

Fig. 8. (a) Observed monsoon onset date measured as the average of monsoon onset date using GPCP and CMAP pentad precipitation. Bias in monsoon onset date in (b) CONT, (c) GLOB, (d) GLOB_A, (e) ELSE, and (f) ASIA with respect to observations.

Figure 1.

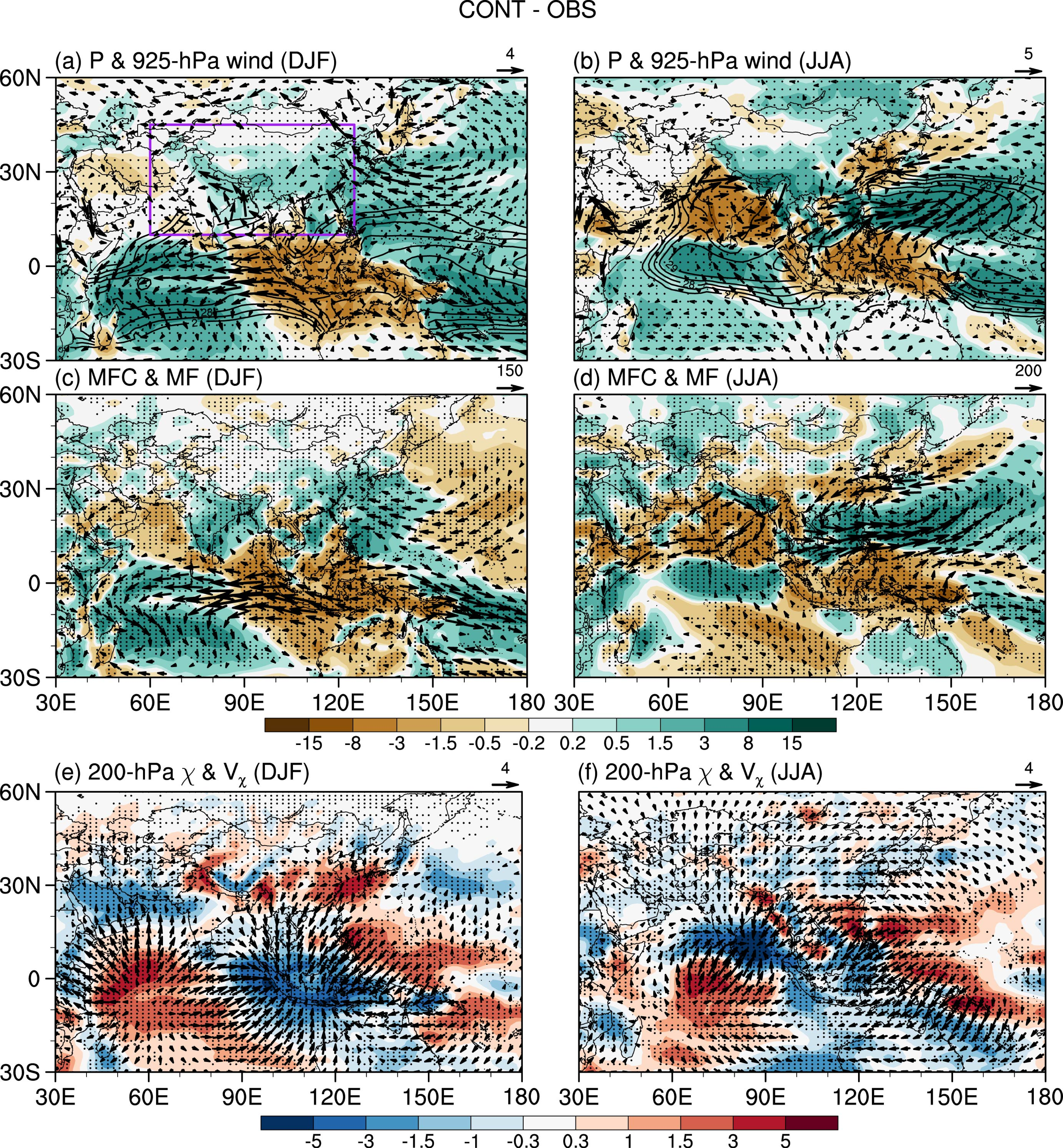
CONT - OBS
(a) P & 925-hPa wind (DJF)
(b) P & 925-hPa wind (JJA)
(c) MFC & MF (DJF)
(d) MFC & MF (JJA)
(e) 200-hPa χ & Vχ (DJF)
(f) 200-hPa χ & Vχ (JJA)
4
5
150
200
60N
30N
0
30S
30E
60E
90E
120E
150E
180
-15 -8 -3 -1.5 -0.5 -0.2 0.2 0.5 1.5 3 8 15
-5 -3 -1.5 -1 -0.3 0.3 1 1.5 3 5

Figure 2.

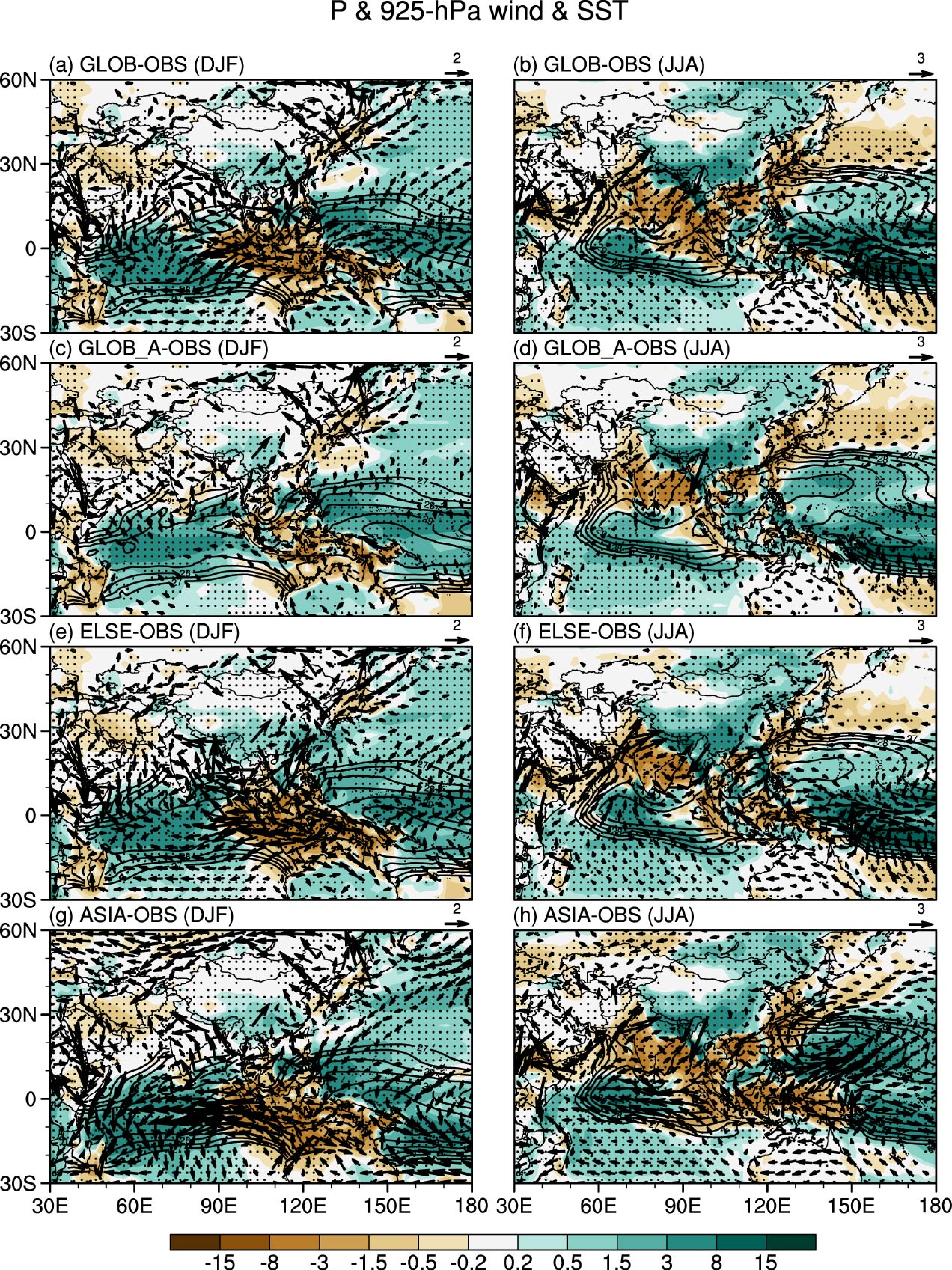

P & 925-hPa wind & SST
(a) GLOB-OBS (DJF)
(b) GLOB-OBS (JJA)
(c) GLOB_A-OBS (DJF)
(d) GLOB_A-OBS (JJA)
(e) ELSE-OBS (DJF)
(f) ELSE-OBS (JJA)
(g) ASIA-OBS (DJF)
(h) ASIA-OBS (JJA)
2
3
60N
30N
0
30S
30E
60E
90E
120E
150E
180
-15 -8 -3 -1.5 -0.5 -0.2 0.2 0.5 1.5 3 8 15

Figure 3.

200-hPa χ & Vχ
(a) GLOB-OBS (DJF)
(b) GLOB-OBS (JJA)
(c) GLOB_A-OBS (DJF)
(d) GLOB_A-OBS (JJA)
(e) ELSE-OBS (DJF)
(f) ELSE-OBS (JJA)
(g) ASIA-OBS (DJF)
(h) ASIA-OBS (JJA)
3
60N
30N
0
30S
30E
60E
90E
120E
150E
180
-5
-3
-1.5
-1
-0.3
0.3
1
1.5
3
5

Figure 4.

GLOB_A-GLOB
(a) P (DJF)
(b) P (JJA)
(c) 200-hPa χ & Vχ (DJF)
(d) 200-hPa χ & Vχ (JJA)
60N
30N
0
30S
30E
60E
90E
120E
150E
180
-15
-8
-3
-1.5
-0.5
-0.2
0.2
0.5
1.5
3
8
15
-5
-3
-1.5
-1
-0.3
0.3
1
1.5
3
5

Figure 5.

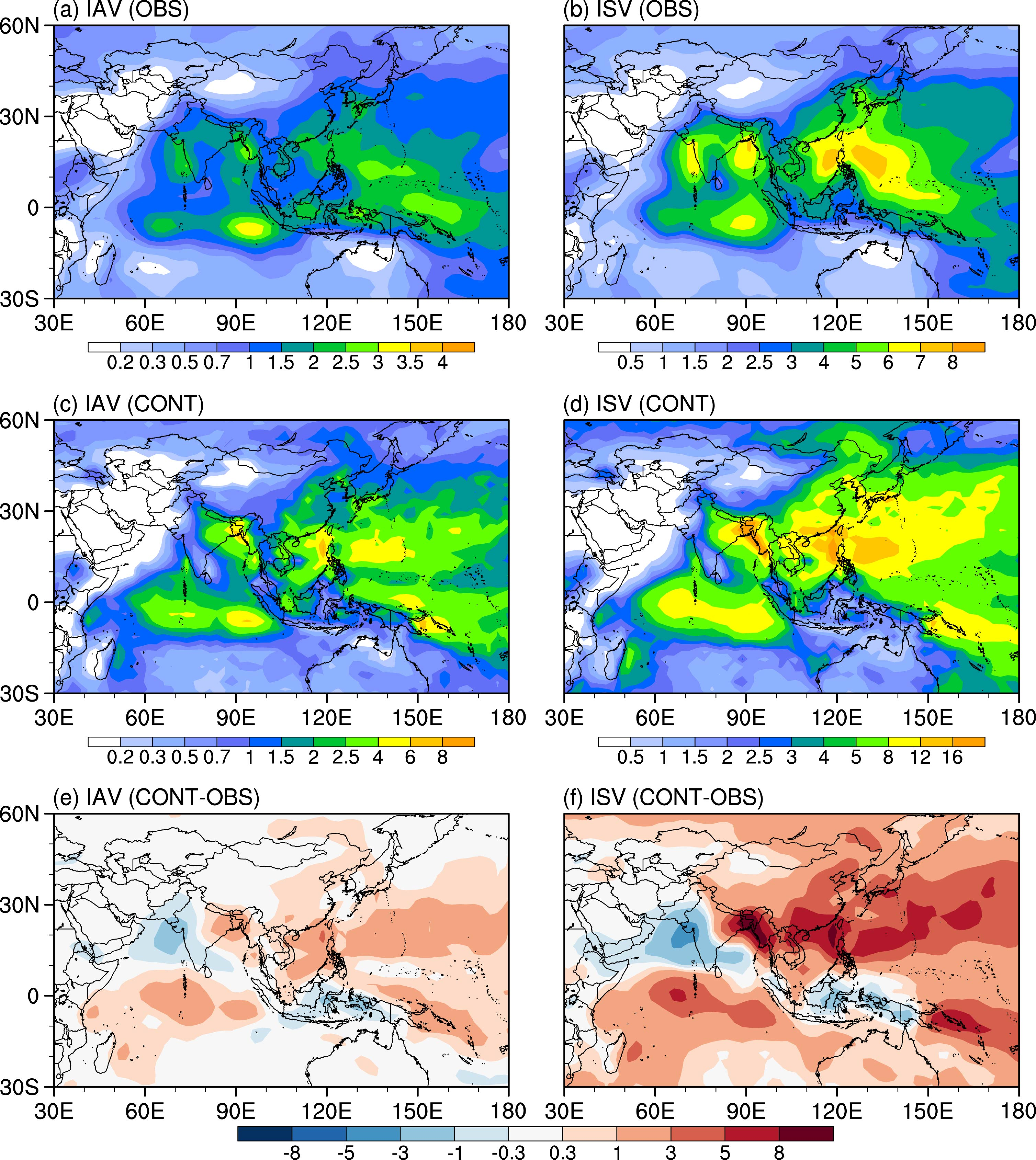

(a) IAV (OBS)
(b) ISV (OBS)
(c) IAV (CONT)
(d) ISV (CONT)
(e) IAV (CONT-OBS)
(f) ISV (CONT-OBS)
60N
30N
0
30S
30E
60E
90E
120E
150E
180
0.2 0.3 0.5 0.7 1 1.5 2 2.5 3 3.5 4
0.5 1 1.5 2 2.5 3 4 5 6 7 8
0.2 0.3 0.5 0.7 1 1.5 2 2.5 4 6 8
0.5 1 1.5 2 2.5 3 4 5 8 12 16
-8 -5 -3 -1 -0.3 0.3 1 3 5 8

Figure 6.

(a) IAV (GLOB-OBS)
(b) ISV (GLOB-OBS)
(c) IAV (GLOB_A-OBS)
(d) ISV (GLOB_A-OBS)
(e) IAV (ELSE-OBS)
(f) ISV (ELSE-OBS)
(g) IAV (ASIA-OBS)
(h) ISV (ASIA-OBS)
60N
30N
0
30S
30E
60E
90E
120E
150E
180
-8
-5
-3
-1
-0.3
0.3
1
3
5
8

Figure 7.

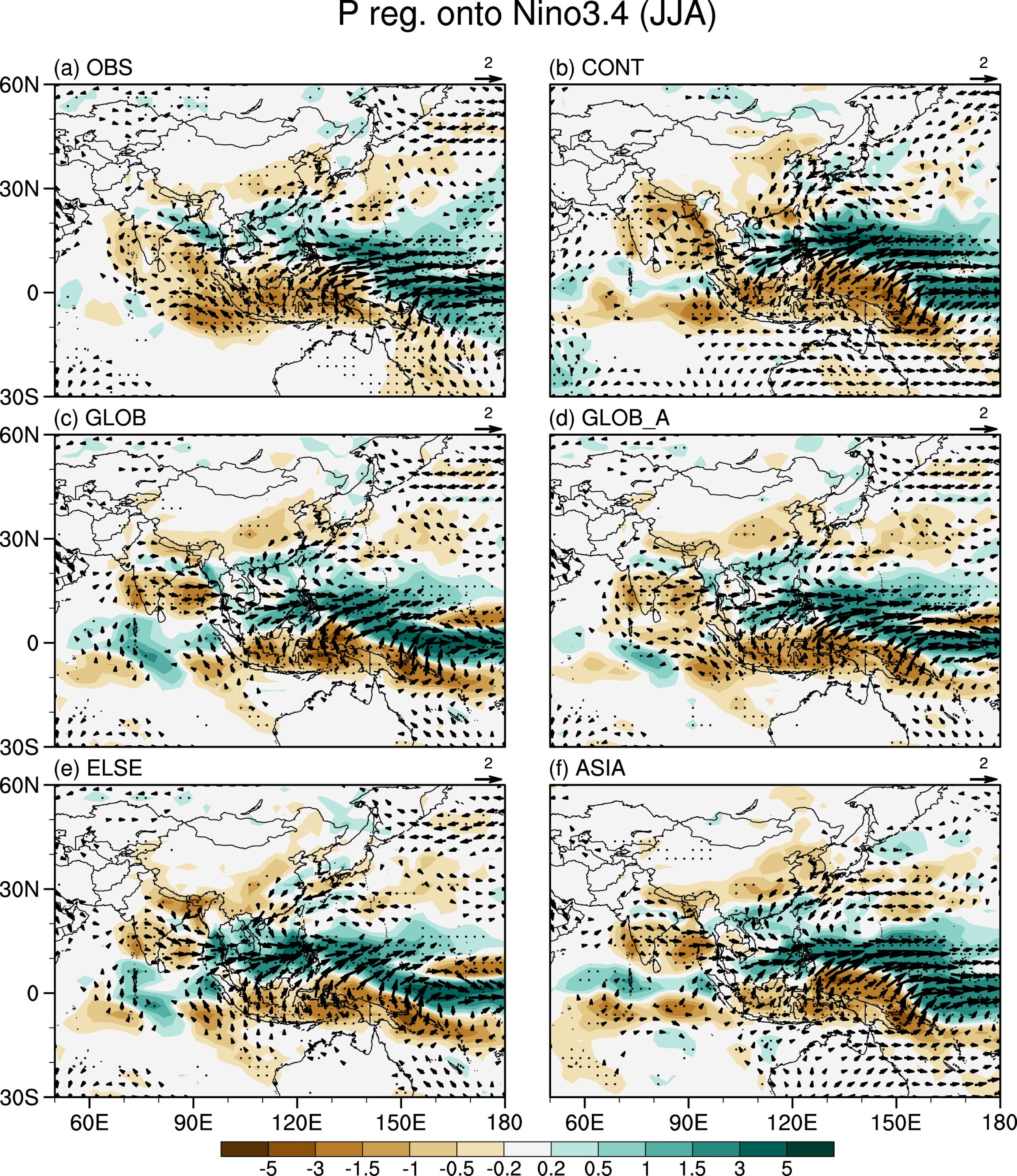
P reg. onto Nino3.4 (JJA)
(a) OBS
(b) CONT
(c) GLOB
(d) GLOB_A
(e) ELSE
(f) ASIA
2
60N
30N
0
30S
60E
90E
120E
150E
180
-5
-3
-1.5
-1
-0.5
-0.2
0.2
0.5
1
1.5
3
5

Figure 8.

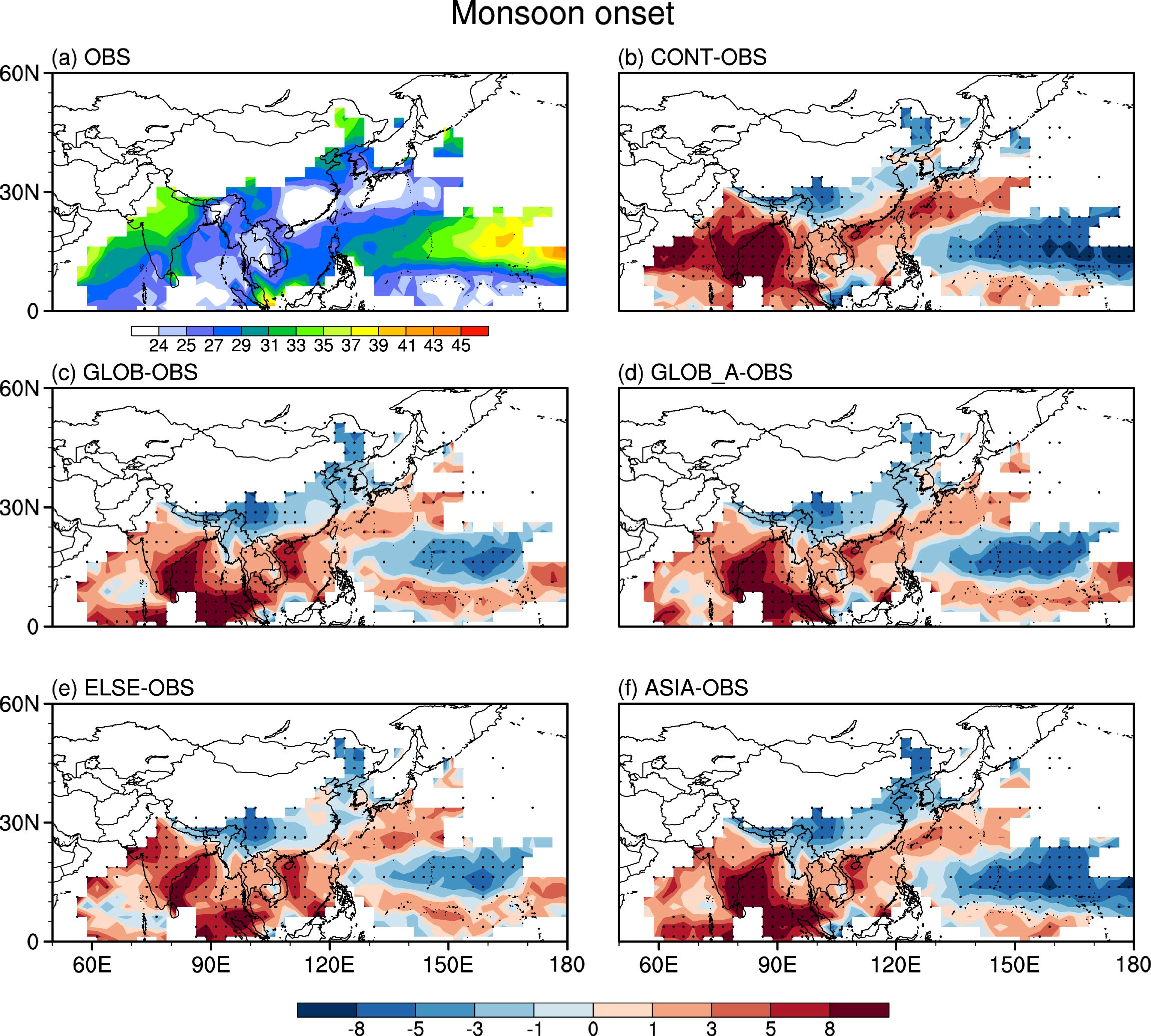
Monsoon onset
(a) OBS
(b) CONT-OBS
(c) GLOB-OBS
(d) GLOB_A-OBS
(e) ELSE-OBS
(f) ASIA-OBS
60N
30N
0
60E
90E
120E
150E
180
24 25 27 29 31 33 35 37 39 41 43 45
-8 -5 -3 -1 0 1 3 5 8